CHEMISTRY OF MATERIALS
Article

Chem. Mater. **2010,** *22,* 2219–2225 2219
DOI:10.1021/cm903492k

Rectangular Nanotubes of Copper Phthalocyanine: Application to a Single Nanotube Transistor

Jin S. Jung, Jin W. Lee, Kihyun Kim, Mi Y. Cho, Seong G. Jo, and Jinsoo Joo*

Department of Physics, Korea University, Seoul 136-713, Korea

Received November 16, 2009. Revised Manuscript Received February 3, 2010

We report on the structural transformation of organic copper phthalocyanine (CuPc) nanowires to hollowed rectangular nanotubes through the use of a hydrothermal process. The CuPc molecules have been chemically self-assembled into a form of nanowires, through reaction with trifluoroacetic acid. The mechanism of the chemical self-assembly for the CuPc nanowires is studied through analyzing the Fourier transform infrared spectra. After the hydrothermal process, it is observed that the α-phase CuPc nanowires are transformed to β-phase CuPc rectangular nanotubes, with crystallinity in the (−101) direction. From X-ray diffraction patterns, the crystallinity of the CuPc nanowires is enhanced by annealing. The optical and electrical characteristics of the β-phase crystalline CuPc rectangular nanotubes are compared with those of α-phase CuPc nanowires, using ultraviolet and visible absorption spectra and current−voltage ($I-V$) characteristics. From the gate field-dependent $I-V$ characteristics for a single nanowire/nanotube transistor, improved device performance in terms of the charge carrier mobility and the current on and off ratio have been observed in the β-phase CuPc crystalline rectangular nanotube compared with the self-assembled α-phase CuPc nanowire, because of the relatively strong $\pi-\pi$ interaction between the CuPc molecules.

Introduction

Optoelectronics using organic semiconductors with a π-conjugated structure have been intensively studied, and their applications have been extended to organic field-effect transistors (OFETs),[1−3] organic photovoltaic cells (OPVCs),[4,5] organic light-emitting diodes (OLEDs),[6,7] and organic phototransistors.[8,9] Organic semiconductors used as active materials have advantages for optoelectronic applications because of their light weight, large area coverage, and ease in processing at low temperatures.

Nanoscience and related technologies based on low-dimensional inorganic nanowires, carbon nanotubes, and organic-based nanostructures have attracted considerable attention over recent years because of their intrinsic low-dimensional nature with well-defined structures.[10−12] Single-crystalline organic-based nanostructures with various physical shapes have been fabricated and have been found to produce fewer defects and no grain boundaries. These findings contribute to the improved intrinsic properties of the nanostructures produced, resulting in the fabrication of high-quality organic-based electronic devices.[13,14] Various organic-based nanostructures using π-conjugated small molecules have been fabricated by using chemical vapor deposition,[15] physical vapor deposition,[16,17] or electrochemical methods.[18,19] Self-assembled polymer nanowires or nanotubes with a π-conjugated structure have also been studied by Wan and other groups.[20−22] The self-assembled nanostructures

*Corresponding author. Phone: +82-2-3290-3103. Fax: +82-2-927-3292. E-mail: jjoo@korea.ac.kr.

(1) Muccini, M. *Nat. Mater.* **2006**, *5*, 605–613.
(2) Briseno, A. L.; Mannsfeld, S. C. B.; Jenekhe, S. A.; Bao, Z.; Xia, Y. *Mater. Today* **2008**, *11*, 38–47.
(3) Briseno, A. L.; Mannsfeld, S. C. B.; Ling, M. M.; Liu, S.; Tseng, R. J.; Reese, C.; Roberts, M. E.; Yang, Y.; Wudl, F.; Bao, Z. *Nature* **2006**, *444*, 913–917.
(4) Perez, M. D.; Borek, C.; Forrest, S. R.; Thompson, M. E. *J. Am. Chem. Soc.* **2009**, *131*, 9281–9286.
(5) Peumans, P.; Uchida, S.; Forrest, S. R. *Nature* **2003**, *425*, 158–162.
(6) Müller, C. D.; Falcou, A.; Reckefuss, N.; Rojahn, M.; Wiederhirn, V.; Rudati, P.; Frohne, H.; Nuyken, O.; Becker, H.; Meerholz, K. *Nature* **2003**, *421*, 829–833.
(7) Williams, E. L.; Haavisto, K.; Li, J.; Jabbour, G. E. *Adv. Mater.* **2007**, *19*, 197–202.
(8) Cho, M. Y.; Kim, S. J.; Han, Y. D.; Park, D. H.; Kim, K. H.; Choi, D. H.; Joo, J. *Adv. Funct. Mater.* **2008**, *18*, 2905–2912.
(9) Tang, Q.; Li, L.; Song, Y.; Liu, Y.; Li, H.; Xu, W.; Liu, Y.; Hu, W.; Zhu, D. *Adv. Mater.* **2007**, *19*, 2624–2628.
(10) Reese, C.; Bao, Z. *Mater. Today* **2007**, *10*, 20–27.
(11) Tang, Q.; Li, H.; Song, Y.; Xu, W.; Hu, W.; Jiang, L.; Liu, Y.; Wang, X.; Zhu, D. *Adv. Mater.* **2006**, *18*, 3010–3014.
(12) Zhao, Y. S.; Fu, H.; Peng, A.; Ma, Y.; Xiao, D.; Yao, J. *Adv. Mater.* **2008**, *20*, 2859–2876.
(13) Briseno, A. L.; Mannsfeld, S. C. B.; Lu, X.; Xiong, Y.; Jenekhe, S. A.; Bao, Z.; Xia, Y. *Nano Lett.* **2007**, *7*, 668–675.
(14) Podzorov, V.; Sysoev, S. E.; Loginova, E.; Pudalov, V. M.; Gershenson, M. E. *Appl. Phys. Lett.* **2003**, *83*, 3504–3506.
(15) Kim, K.; Kim, B. H.; Joo, S.-H.; Park, J.-S.; Joo, J.; Jin, J.-I. *Adv. Mater.* **2005**, *17*, 464–468.
(16) Kloc, Ch.; Simpkins, P. G.; Siegrist, T.; Laudise, R. A. *J. Cryst. Growth* **1997**, *182*, 416–427.
(17) Tang, Q.; Jiang, L.; Tong, Y.; Li, H.; Liu, Y.; Wang, Z.; Hu, W.; Liu, Y.; Zhu, D. *Adv. Mater.* **2008**, *20*, 2947–2951.
(18) Martin, C. R. *Science* **1994**, *266*, 1961–1966.
(19) Penner, R. M.; Martin, C. R. *J. Electrochem. Soc.* **1986**, *133*, 2206–2207.
(20) Xin, H.; Kim, F. S.; Jenekhe, S. A. *J. Am. Chem. Soc.* **2008**, *130*, 5424–5425.
(21) Zhang, L.; Long, Y.; Chen, Z.; Wan, M. *Adv. Funct. Mater.* **2004**, *14*, 693–698.
(22) Schenning, A. P. H. J.; Meijer, E. W. *Chem. Commun.* **2005**, *26*, 3245–3258.

Published on Web 02/16/2010

of the organic small molecules[23,24] through a relatively strong $\pi-\pi$ stacking could contribute to enhanced thermal stabilities and relatively high charge-carrier mobilities in electronic devices.[17,25]

Organic metal phthalocyanine (MPc) molecules, such as copper phthalocyanine (CuPc), zinc phthalocyanine (ZnPc), etc., consisting of a central metal atom bound to the π-conjugated ligands, have been applied to active materials for fabricating OLEDs,[26] OFETs,[11] OPVCs,[4] and various other sensors,[27] because of their environmental stability and excellent photoresponsive characteristics. Recently, Tang and co-workers have synthesized a number of nanostructures, including nanoribbons of MPc molecules, by using the physical vapor deposition method.[17] Forrest and co-workers have studied the bulk heterojunction photovoltaic cells, using vapor-phase deposition grown and controlled CuPc/3,4,9,10-perylenetetracarboxylic bis-benzimidazole.[5] And Jenekhe and co-workers reported the ambipolar OTFTs using the blends of benzobisimidazobenzophenanthroline (BBL) and CuPc.[28] However, the systematic study of solution-based chemically self-assembled CuPc nanowires and their transformed nanostructures, and optoelectronic characteristics have not yet been studied in any significant detail.

This study reports that CuPc molecules have been chemically self-assembled into a form of nanowires, through reaction with trifluoroacetic acid (CF_3COOH). After a hydrothermal process, it is observed that α-phase CuPc nanowires are transformed to high crystalline β-phase CuPc hollowed rectangular nanotubes. The charge carrier mobility (μ) and the current on and off ratio ($I_{on/off}$) of a single nanotube transistor using the β-phase CuPc crystalline rectangular nanotube have been enhanced through the highly crystalline structure and relatively strong $\pi-\pi$ interaction between the CuPc molecules.

Experimental Studies

Synthesis. The CuPc powder from Sigma-Aldrich Co., is used without further purification; the CuPc (1×10^{-4} M) powders are dispersed in chloroform ($CHCl_3$) solution, using an ultrasonic cleaner for 10 min. The CF_3COOH (1.754×10^{-4} M) is added and mixed with the solution by using a magnetic stirrer for 5 h. The CuPc molecules are then chemically self-assembled into a form of nanowires that are then filtered and dried for 24 h. For the fabrication of the CuPc rectangular shaped nanotubes, the self-assembled CuPc nanowires dispersed in methyl alcohol are placed in a hydrothermal chamber (Parr Instrument acid digestion bombs, 4744 general purpose bomb) and heated in a vacuum oven at 180 °C in 1×10^{-3} Torr for 10 h. After the hydrothermal process, the chamber containing the samples is naturally cooled in a vacuum oven for 12 h. The additional annealing process of the as-grown (i.e., self-assembled) or hydrothermal treated CuPc nanostructures have been performed onto a glass substrate in a vacuum oven at 180 °C in 1×10^{-3} Torr for 10 h.

Measurements. For the scanning electron microscope (SEM) and high resolution transmission electron microscope (HR-TEM) images, the Hitachi S-4300 and the JEOL JEM-2000EXII systems have been used, respectively. The XRD patterns are measured by using an XRD [PANalytical X'Pert PRO, Cu−K_α radiation (λ = 1.54 Å)]. For the XRD experiments, the samples are placed on a quartz substrate. The chemical structures of the CuPc nanostructures are analyzed using the Fourier transform infrared (FT-IR) spectra (obtained using the PERKIN ELMER spectrum GX FT-IR system). To study the optical properties, ultraviolet and visible (UV/vis) absorption spectra of the CuPc nanostructures dispersed in methyl alcohol are measured by using an HP-8453 spectrometer. For photoresponsive $I-V$ characteristic curves, the wavelength and power of the incident light are 633 nm and 5−6 mW cm^{-2}, respectively. The optical powers are measured using an optical-power meter (Thorlabs PM120) connected to a sensor (Thorlabs S130A). For obtaining the photoresponsive electrical characteristics, 4−5 strands of the nanowires or nanotubes are placed onto the source-drain electrodes. To investigate the gate field-dependent charge transport properties, the doped p-type Si wafer (R = 0.001−0.003 Ω cm) and the thermally grown SiO_2 layer are used as the gate electrode and the dielectric layer, respectively. The thickness and dielectric constant (ε_r) of the SiO_2 layer are ∼250 nm and ∼3.9, respectively. Using conventional photolithography, gold (Au) source and drain electrodes are patterned with a length and width of ∼5−20 and 1500 μm, respectively, and for better adhesion, a Ti layer of thickness ∼5 nm is deposited before the deposition of the Au electrodes. Devices are treated with ozone during 300 s and are spin-coated with hexamethyldisilazane (HMDS) at 4500 rpm during 75 s for a better adhesion between the hydrophobic organic CuPc nanowire or nanotube and the relatively hydrophilic SiO_2 layer. The single strand of CuPc nanostructures are placed onto the Au electrodes, and coated with poly (methylmethacrylate) (PMMA) solution at 4500 rpm during 75 s, before a modest pressure is applied. The PMMA coating can assist the homogeneous pressure on the sample for better electrical contact, and prevents the oxidation of the samples.[29] Ten different devices have been fabricated to measure the gate field-dependent $I-V$ characteristics of the CuPc nanostructures. And the leakage currents of the devices are measured to be 3.50 (± 1.19) × 10^{-10} A.

Results and Discussion

Self-Assembled CuPc Nanowires and Their Transformed Rectangular Nanotubes. Figure 1 shows the SEM and HR-TEM images of the self-assembled (i.e., as-grown) CuPc nanowires, the annealed CuPc nanowires, the hydrothermal treated CuPc nanotubes, and the hydrothermal process followed by the annealed CuPc nanotubes. The diameters and lengths of the self-assembled CuPc nanowires are 300−800 nm and 20−50 μm, respectively, as shown in Figure 1a. As the CuPc molecules are chemically interacted

(23) Zang, L.; Che, Y.; Moore, J. S. *Acc. Chem. Res.* **2008**, *41*, 1596–1608.
(24) Wang, Z.; Medforth, C. J.; Shelnutt, J. A. *J. Am. Chem. Soc.* **2004**, *126*, 15954–15955.
(25) Ahmed, E.; Briseno, A. L.; Xia, Y.; Jenekhe, S. A. *J. Am. Chem. Soc.* **2008**, *130*, 1118–1119.
(26) Kao, P.-C.; Chu, S.Y.; Liu, S.-J.; You, Z.-X.; Chuang, C.-A. *J. Electrochem. Soc.* **2006**, *153*, H122–H126.
(27) Bohrer, F. I.; Colesniuc, C. N.; Park, J.; Ruidiaz, M. E.; Schuller, I. K.; Kummel, A. C.; Trogler, W. C. *J. Am. Chem. Soc.* **2009**, *131*, 478–485.
(28) Babel, A.; Wind, J. D.; Jenekhe, S. A. *Adv. Funct. Mater.* **2004**, *14*, 891–898.
(29) Lee, J. Y.; Roth, S.; Park, Y. W. *Appl. Phys. Lett.* **2006**, *88*, 252106−1–252106−3.

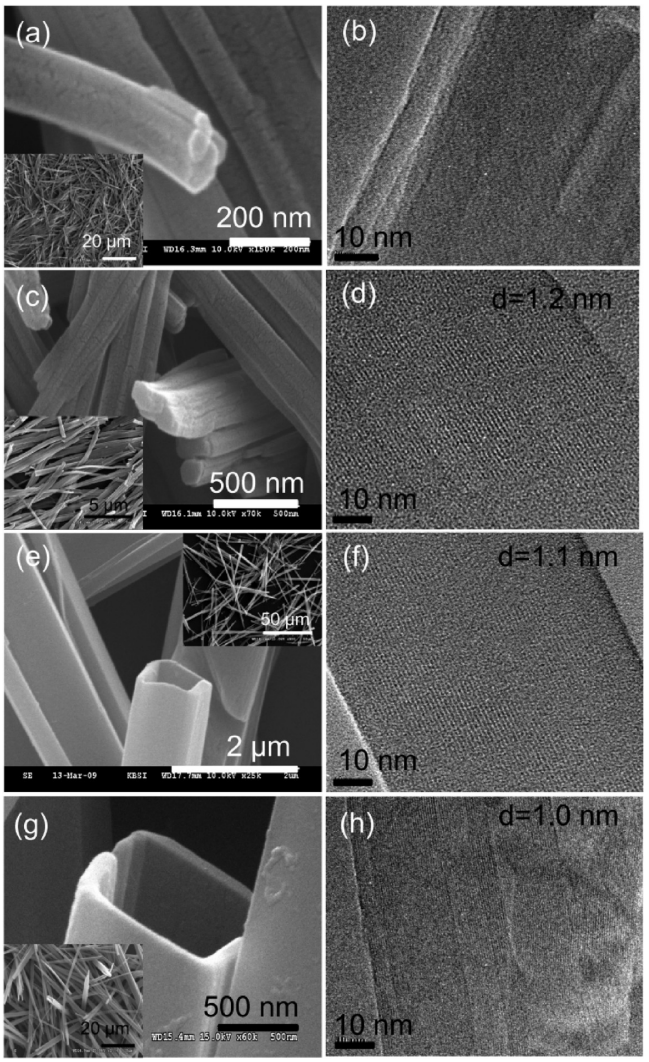

Figure 1. (a, b) SEM and HR-TEM images of the self-assembled CuPc nanowires, respectively. (c, d) SEM and HR-TEM images of the annealed CuPc nanowires, respectively. (e, f) SEM and HR-TEM images of the hydrothermal treated CuPc hollowed rectangular nanotubes, respectively. (g, h) SEM and HR-TEM images of hydrothermal process followed by the annealed CuPc hollowed rectangular nanotubes, respectively. Insets of a, c, e, and g: SEM images of the side view of the CuPc nanowires and rectangular nanotubes.

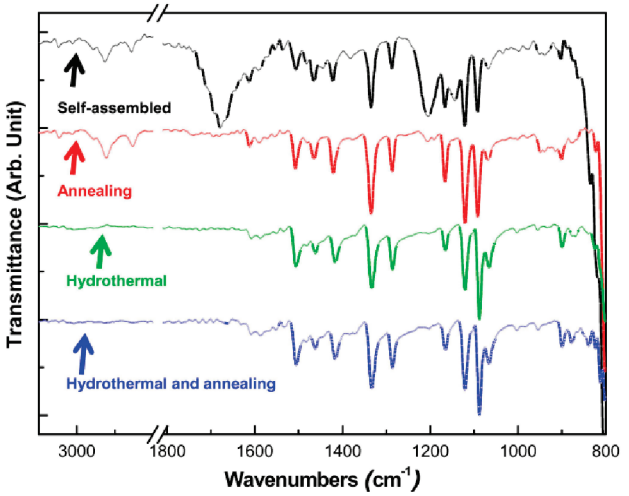

Figure 2. FT-IR spectra of the CuPc nanowires and the CuPc rectangular nanotubes.

with the CF_3COO^- ions, causing the CuPc molecules to be self-assembled into the form of nanowires (see the analysis of the FT-IR spectra in Figure 2 for further details). Figure 1b shows the HR-TEM image of the self-assembled CuPc nanowire where a relatively amorphotic phase is observed, i.e., no periodic patterns in the HR-TEM image. Figure 1c shows the SEM image of the annealed CuPc nanowires and the diameters and lengths of the annealed CuPc nanowires are 300−500 nm and 20−50 μm, respectively. After the annealing process, the diameters of the CuPc nanowires become smaller. Figure 1d shows a HR-TEM image of the annealed CuPc nanowire. From this HR-TEM image, the periodic stripe pattern implies a crystalline structure of the annealed CuPc nanowires, and the interlayer *d*-space of the annealed CuPc nanowire can be estimated to be ~1.2 nm, which is determined by digital micrograph software (Gatan-TEM imaging) measurement, as shown in Figure 1d. This indicates an increase in the crystallinity of the CuPc nanowires after the annealing process. It is noted that the inside of the CuPc nanowires is filled, as shown in images a and c in Figure 1. After the hydrothermal treatment of the self-assembled CuPc nanowires, the physical shape of the CuPc nanowires is dramatically changed to the hollowed rectangular nanotubes (i.e., an empty nanometer size rectangular waveguide), as shown in images e and g in Figure 1. The lengths and widths of the CuPc rectangular nanotubes increase to 50−100 μm and 500 nm to 2.8 μm, respectively. The wall thickness of the CuPc rectangular nanotubes is estimated to be ~100 nm. From the HR-TEM images, as shown in images f and h in Figure 1, the interlayer *d*-space of the hydrothermal and the hydrothermal process followed by annealed CuPc nanotubes, are estimated to be ~1.1 and ~1.0 nm, respectively. These results indicate the structural transformation of the CuPc nanowires to the hollowed rectangular nanotubes through the hydrothermal process.

Self-Assembly Mechanism of CuPc Nanowires. Figure 2 shows the FT-IR spectra of the self-assembled CuPc nanowires and hydrothermal and/or annealed CuPc nanostructures. The IR characteristic peaks due to the vibration mode of Cu−N bonding and the C=N−C at bridge sites are observed at 1166 and 1287 (and 1334) cm^{-1}, respectively. For the self-assembled, hydrothermal, and/or annealed CuPc nanowires and nanotubes, the IR characteristic peaks related to the CuPc molecule have the same positions. The detailed assignments of the IR characteristic peaks are listed in Table 1 (see the Supporting Information). The CuPc molecular structure has been confirmed from the FT-IR spectra.[30] However, only for the self-assembled CuPc nanowires are the additional IR peaks observed at 1144, 1384, 1444, and 1679 cm^{-1}, because of the CF_3COOH molecules. The peak at 1144 cm^{-1} corresponds to the C−F stretching modes and the peaks at 1384 and 1444 cm^{-1} indicate the C−O deformation mode. The peak at 1679 cm^{-1} is

(30) Kato, H.; Takemura, S.; Watanabe, Y.; Ishii, A.; Tsuchida, I.; Akai, Y.; Sugiyama, T.; Hiramatsu, T.; Nanba, N.; Nishikawa, O.; Taniguchi, M. *J. Vac. Sci. Technol., A* **2007**, *25*, 1147–1151.

assigned to the C=O stretching modes. These results imply that the CF_3COO^- ions remain in the self-assembled CuPc nanowires, which induce the chemical self-assembly of the CuPc molecules. The CF_3COO^- ions interact with the Cu^{2+} ions of the CuPc molecules in the $CHCl_3$ solution, and play a bridging role for the self-assembly of the CuPc molecules into the form of nanowires. The remaining CF_3COO^- ions in the self-assembled CuPc nanowires can be mainly placed between the CuPc molecules, and so reduce the $\pi-\pi$ interaction of the CuPc molecules. The IR peaks of the CF_3COOH molecules disappear after the hydrothermal or annealing process, except for the O−H related peaks, as listed in Table 1 (see the Supporting Information) and shown in Figure 2. The IR peaks of the O−H related modes are observed at 1204, 2856, 2926, and 3048 cm^{-1}, as shown in Figure 2.[31] These O−H mode related IR peaks disappear after the hydrothermal process. Based on the analysis of the FT-IR spectra, it is suggested that the CF_3COO^- ions contribute to the chemical self-assembly of the CuPc molecules, and are removed through the hydrothermal and/or annealing processes.

Structural and Optical Characteristics of CuPc Nanowires and Rectangular Nanotubes. Figure 3a shows the XRD patterns of the self-assembled CuPc nanowires and their annealed samples. The XRD peaks of the self-assembled and annealed CuPc nanowires have the same positions, as shown in Figure 3a. Two crystalline peaks at 6.76 and 7.301° of the CuPc nanowires indicate the α-phase molecular stacking structures.[32] For the self-assembled CuPc nanowires, the intensities of the XRD peaks are relatively weaker than those of the annealed CuPc nanowires, suggesting the relatively amorphortic α-phase CuPc nanowires, because the CF_3COO^- ions remain between the CuPc molecules, as discussed in the FT-IR spectra of Figure 2. This contributes to the weakness of the $\pi-\pi$ stacking of the CuPc molecules and interrupt the crystalline formation. However, after the annealing process of the self-assembled CuPc nanowires, the CF_3COO^- ions are removed, resulting in the increase of the crystallinity and the $\pi-\pi$ stacking. These results agree with those of the HR-TEM images in Figures 1b,d. Figure 3b shows the XRD patterns of the hydrothermal and hydrothermal process followed by the annealed CuPc hollowed rectangular nanotubes. The XRD crystalline peaks are observed at 7.08 and 9.25°, which indicate the β-phase CuPc molecular stacking structures, as shown in the inset of Figure 3b.[33] It is noted that the tilted angles of the CuPc molecules in the α- and β-phases are at 26.5 and 45.8°, respectively.[34] The hydrothermal process induces the transformation of the α-phase CuPc nanowires to

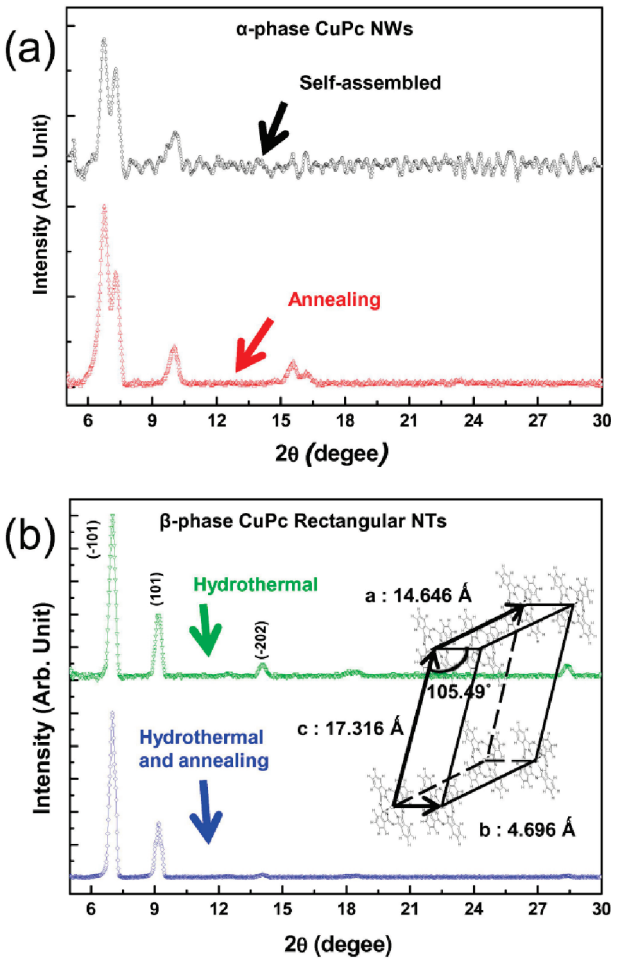

Figure 3. (a) XRD patterns of the self-assembled and the annealed CuPc nanowires. (b) XRD patterns of the hydrothermal and hydrothermal process followed by the annealed CuPc rectangular nanotubes. Inset: Monoclinic crystalline structure of the β-phase CuPc hollowed rectangular nanotubes.

the β-phase CuPc hollowed rectangular nanotubes. The CuPc rectangular nanotubes treated with both hydrothermal and annealing processes also have the β-phase stacking of the CuPc molecules. Using Bragg's law ($2d\sin\theta = n\lambda$) for the XRD patterns, the lattice constants of the β-phase CuPc hollowed rectangular nanotubes are estimated to be a = 14.646 Å, b = 4.696 Å, and c = 17.316 Å, and the angles are $\alpha = \gamma = 90°$ and $\beta = 105.49°$, indicating monoclinic structures. For the hydrothermal and annealed CuPc nanotubes, the CuPc molecules are well-aligned along the direction of $(\bar{1}01)$, corresponding to a relatively high XRD peak at 7.08°, as shown in Figure 3b. During the hydrothermal process, with the conditions of high pressure and high temperature in the closed hydrothermal chamber, not only the CF_3COOH molecules are removed but also the CuPc molecules are more tilted and closely packed in the energetically most stable states.

The CuPc molecule has 4-membered phthaloimino groups around the Cu atom. The 4-membered phthaloimino groups as negative charged ligands and the Cu atom as positive charge are made up for the electric dipole.[35]

(31) Fuson, N.; Josien, M. -L.; Jones, E. A.; Lawson, J. R. *J. Chem. Phys.* **1952**, *20*, 1627–1634.
(32) Ballirano, P.; Caminiti, R.; Ercolani, C.; Maras, A.; Orr, M. A. *J. Am. Chem. Soc.* **1998**, *120*, 12798–12807.
(33) Xiao, K.; Li, R.; Tao, J.; Payzant, E. A.; Ivanov, I. N.; Puretzky, A. A.; Hu, W.; Geohegan, D. B. *Adv. Funct. Mater.* **2009**, *19*, 3776–3780.
(34) *Phthalocyanine: Properties and Applications*; Snow, A. W., Barger, W. R., Eds.; VCH: New York, 1989; p 362.
(35) Cho, N.-S.; Kim, K.-H.; Hahn, C.-S. *J. Korean Chem. Soc.* **1972**, *16*, 378–384.

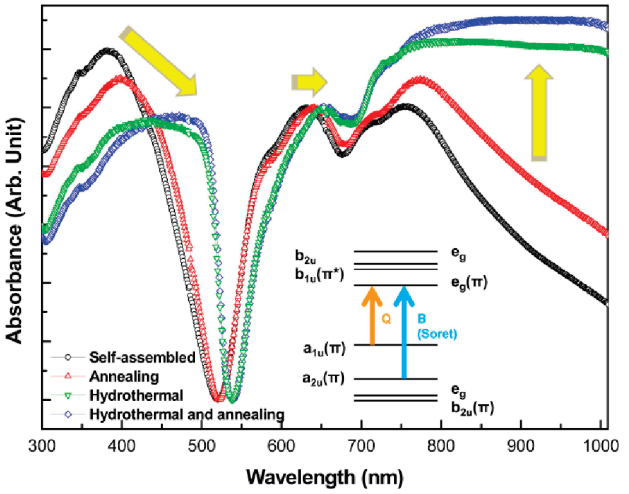

Figure 4. Normalized UV/vis absorption spectra of the self-assembled CuPc nanowires and their transformed nanostructures after the hydrothermal and/or annealing process. Inset: HOMO and LUMO levels of CuPc molecule.

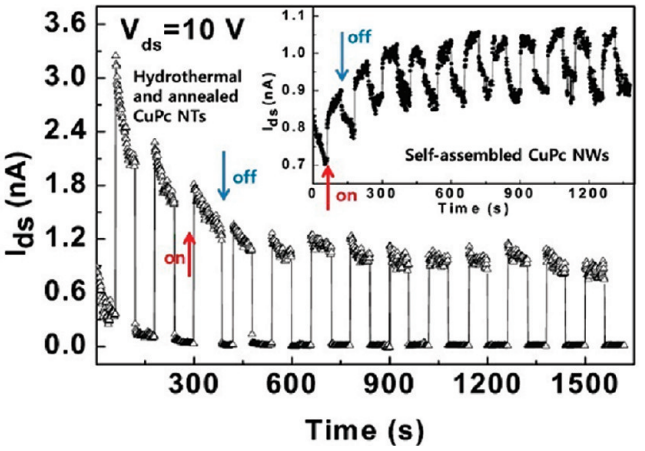

Figure 5. Current (I_{light}/I_{dark}) switching performance of the β-phase CuPc rectangular nanotubes with and without light illumination (λ = 633 nm) in vacuum at RT. Inset: Current (I_{light}/I_{dark}) switching performance of the α-phase CuPc nanowires with and without light illumination.

Because of the weak interaction between the π-orbitals along the π-conjugated path in the 4-membered phthaloimino groups and the delocalized d-orbital of Cu atoms, the CuPc molecules have two levels of HOMO (π-orbitals) and LUMO (π*-orbitals).[36] These induce the UV/vis absorption characteristic bands, as shown in the inset of Figure 4. Figure 4 shows the normalized UV/vis absorption spectra of the self-assembled CuPc nanowires and their transformed nanostructures after the hydrothermal and/or annealing process.

The UV/vis absorption main peaks of CuPc nanowires are observed at 382 and 630 nm, as shown in Figure 4. The UV/vis absorption peaks at 382 and 630 nm correspond to the Soret-band and the Q-band, respectively.[37] The Soret-band (or B-band) is the strong absorption band in the blue region (250−500 nm), whereas the Q-band is a relatively weak absorption band (600−800 nm). The UV/vis absorption peak in the Q-band is divided into two peaks at ~630 and ~750 nm by Davydov splitting. The window region of the CuPc nanowires is observed at ~539 nm. The broad UV/vis absorption bands in the 800−1500 nm region are related to the free charge carrier tail due to the delocalized π-electrons.[38] After the hydrothermal process of the α-phase CuPc nanowires, the UV/vis absorption peaks corresponding to the Soret-band and Q-band at 382 and 630 nm shifted to longer wavelengths at 450 and 653 nm, respectively, because of the structural modification, as shown in Figure 4. The intensity of the UV/vis absorption peak at 382 nm relatively decreases and the red-shift of the Soret-band implies that the gap of $\pi-\pi$* transition also decreases. This suggests the delocalization of the π-electrons along the π-conjugated path in the 4-membered phthaloimino groups, after the hydrothermal process. The decrease of the UV/vis absorption peak intensity at 382 nm means that the Soret-band $\pi-\pi$* transition might easily occur with the longer wavelength light absorption, which could be applied to optoelectronic devices using the hydrothermal treated CuPc rectangular nanotubes. The UV/vis absorption peak at the long wavelength region (≥800 nm) of the Q-band increases as shown in Figure 4 because the number of the delocalized π-electrons in the intraband increases after the hydrothermal process. Therefore, it is expected that the charge transport property along the direction of the $\pi-\pi$ stacking of the hydrothermal treated β-phase CuPc rectangular nanotubes is better than those of the α-phase CuPc nanowires.

Photoresponsive Electrical Characteristics. Figure 5 and its inset show the light/dark current (I_{light}/I_{dark}) switching performance with the irradiating light (λ = 633 nm, power = 5−6 mW cm^{-2}) at a constant drain voltage (V_{ds} = 10 V) for the CuPc nanotubes and nanowires, respectively, in a vacuum at room temperature (RT). When the nanotubes and nanowires are exposed to the light illumination, both current levels are increased, as shown in Figure 5 and its inset, indicating active photoresponsive electrical characteristics. In the case of the α-phase CuPc nanowires, $V_{ds}(t)$ is increased only slightly during the first 400 s and then becomes saturated. For the β-phase crystalline CuPc rectangular nanotubes $V_{ds}(t)$ is decreased during the first 400 s and then saturated. Similar results have been observed for the five different devices.

The high and low current states are repeated when the light is turned on and off, respectively, during more than 20 min. The ratio of I_{light}/I_{dark} is 15.8 ± 11.1 for the β-phase crystalline CuPc rectangular nanotubes and 3.62 ± 0.63 for the α-phase CuPc nanowires. The ratio of I_{light}/I_{dark} of the β-phase crystalline CuPc rectangular nanotubes is ~4 times higher than that of the α-phase CuPc nanowires. The maximum value of the ratio of I_{light}/I_{dark} of the β-phase crystalline CuPc rectangular nanotubes is 36.4 and that of the α-phase CuPc nanowires is 4.39. Therefore, the β-phase crystalline CuPc rectangular

(36) Hashimoto, T.; Choe, Y.-K.; Nakano, H.; Hirao, K. *J. Phys. Chem. A* **1999**, *103*, 1894–1904.
(37) Edwards, L.; Gouterman, M. *J. Mol. Spectrosc.* **1970**, *33*, 292–310.
(38) Zheng, W.; Min, Y.; MacDiarmid, A. G.; Angelopoulos, M.; Liao, Y.-H.; Epstein, A. J. *Synth. Met.* **1997**, *84*, 63–64.

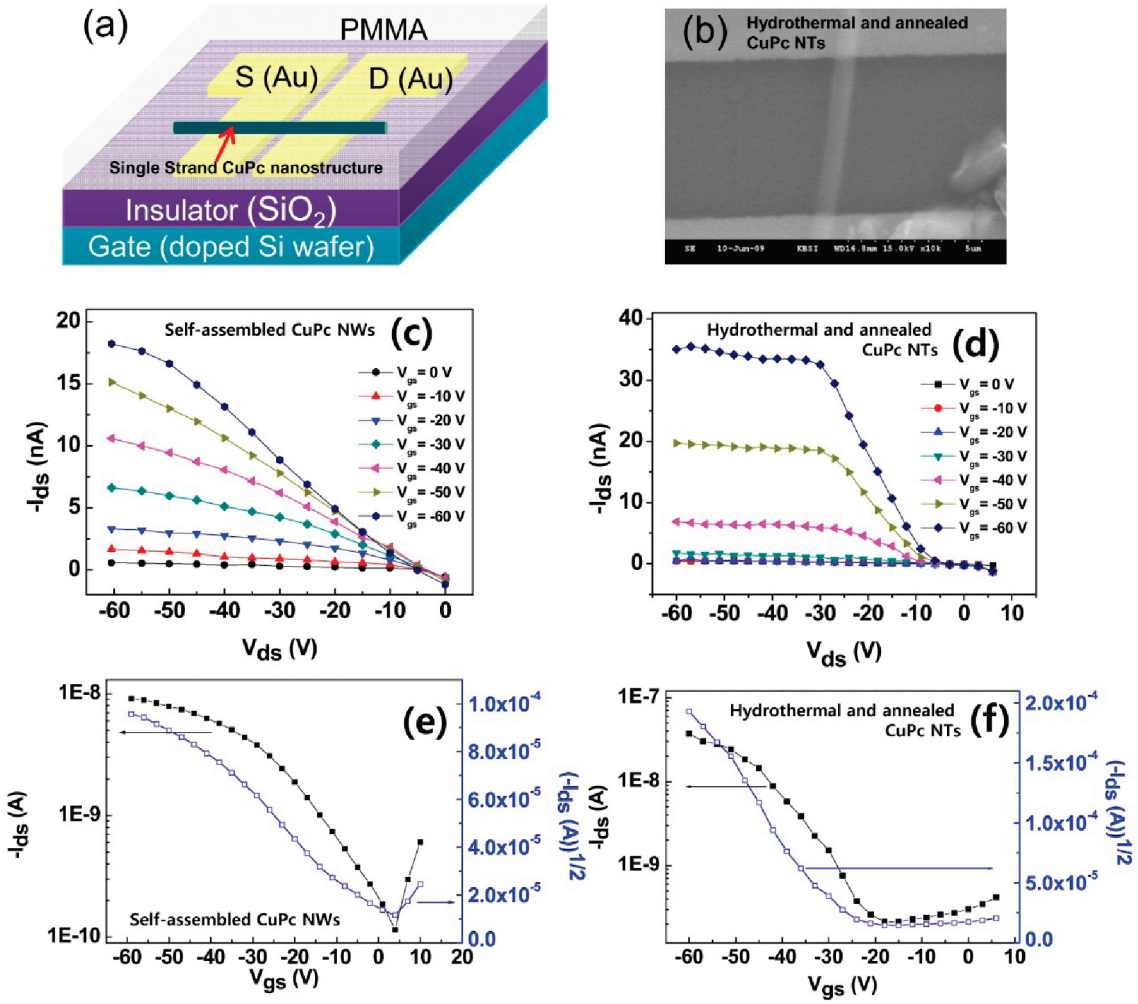

Figure 6. (a) Schematic illustration of a single-strand transistor. (b) SEM image of single-strand transistor using CuPc nanotube. (c) The $I_{ds}-V_{ds}$ characteristic curves with various V_g values of the α-phase CuPc single nanowire-based OFET devices. (d) The $I_{ds}-V_{ds}$ characteristic curves with various V_g values of the β-phase CuPc single rectangular nanotube-based OFET devices. (e) $I_{ds}-V_g$ and $(-I_{ds})^{1/2}-V_g$ characteristic curves of the α-phase CuPc single nanowire-based OFET devices. (f) $I_{ds}-V_g$ and $(-I_{ds})^{1/2}-V_g$ characteristic curves of the β-phase CuPc single rectangular nanotube-based OFET devices.

nanotubes have a relatively higher photosensitive current than the self-assembled α-phase CuPc nanowires. This originates from the relatively strong cofacial π-stacking interaction in the *b*-direction of the CuPc molecules for the hydrothermal process followed by annealed β-phase CuPc rectangular nanotubes.

Gate-Field-Dependent Electrical Characteristics for a Single Nanowire/Nanotube Transistor. Figure 6 shows the gate-field-dependent $I-V$ characteristic curves for transistors using the self-assembled α-phase CuPc single nanowire and the β-phase CuPc single rectangular nanotube. The experimental conditions and device patterns are identical in order to achieve a quantitative comparison. Panels a and b in Figure 6 show the schematic illustration of a single nanowire/nanotube transistor and the SEM image of the real field-effect transistor (FET) device, respectively. Figure 6c−f shows the FET performance of a single strand of the β-phase crystalline CuPc rectangular nanotube and of the α-phase CuPc nanowire in a vacuum condition. It is observed that both devices show typical *p*-type characteristics, in which the negative I_{ds} increases with negatively increasing V_g, as shown in Figures 6c and 6d. The amplification and saturation of the $-I_{ds}$ is clearly observed by applying $-V_g$ for both OFETs, as shown in panels c and d in Figure 6. Panels e and f in Figure 6 show the source-drain current characteristic curves as a function of the gate bias ($I_{ds}-V_g$) when the constant drain voltage, $V_{ds} = -30$ V. The charge carrier mobility (μ) of the OFETs can be estimated by using the equation in the saturation region, $I_{ds} = W\mu C_i(V_g - V_{th})^2/2L$, where the L (5−24 μm) is the channel length (i.e., the sample length between source and drain electrodes), W (0.5−2.8 μm) is the channel width (i.e., the width of single nanostructure), V_{th} is the threshold voltage, and C_i (1.381×10^{-8} Fcm^{-2}) is the capacitance of the gate dielectric per unit area. μ, the ratio of the maximum and minimum values of I_{ds}, the current on/off ratio ($I_{on/off}$), and the threshold voltage (V_{th}) are calculated using the results of panels e and f in Figure 6. The $I_{on/off}$ and V_{th} of the β-phase CuPc single rectangular nanotube-based OFETs are 1×10^3 and -13.5 ± 4.92 V, respectively, whereas those of the α-phase CuPc single nanowire-based OFETs are 1×10^2 and 45.7 ± 35.0 V, respectively. The $I_{on/off}$ of the β-phase CuPc single rectangular nanotube-based OFETs is about 10 times higher than that of the CuPc single nanowire-based OFETs.

From the slope of $(-I_{ds})^{1/2}$ versus V_g, the μ of the β-phase CuPc single rectangular nanotube-based OFETs is estimated to be 1.73 ($\pm$ 1.92) $\times$ 10^{-2} cm^2 V^{-1} s^{-1}, and that of the α-phase CuPc single nanowire-based OFETs is 2.21 ($\pm$ 1.61) $\times$ 10^{-3} cm^2 V^{-1} s^{-1}. The average value of μ's and their standard deviation have been obtained from ten different OFET devices. The averaged μ of the β-phase CuPc single rectangular nanotube-based OFETs is approximately 8 times higher than that of the α-phase CuPc single nanowire ones. It is noted that the maximum μ of the β-phase CuPc single rectangular nanotube-based OFETs is 6.64 $\times$ 10^{-2} cm^2 V^{-1} s^{-1} and that of the α-phase CuPc single nanowire-based OFETs is 5.70 $\times$ 10^{-3} cm^2 V^{-1} s^{-1}. These results suggest that the β-phase CuPc rectangular nanotubes have an improved charge transport nature in comparison to the self-assembled α-phase CuPc nanowires due to the highly crystalline structure and relatively strong $\pi-\pi$ interaction of the CuPc molecules.

It is noted that the μ values of the α-phase CuPc single-nanowire- and β-phase CuPc single-nanotube-based OFETs are lower than those of the α-phase CuPc single-crystal nanowire-based OFETs reported by Xiao's group[33] and of the β-phase CuPc single-crystalline nanoribbon-based OFETs reported by Tang and co-workers.[11] Their CuPc single crystalline nanowires and nanoribbons were fabricated by using the organic vapor deposition method. In our study, the solution-based chemically self-assembled α-phase CuPc nanowires have not perfect crystalline structure due to the existence of CF_3COO^- ions, supported by FT-IR spectra and XRD patterns (Figures 2 and 3a). However, the β-phase CuPc nanotubes induced by the hydrothermal process consist with only CuPc molecules and have better crystalline structure. Comparing with the μ values of the previous reports,[11,33] the lower μ values of the β-phase CuPc single rectangular nanotube-based OFETs studied here may be due to the relatively higher contact resistance because of the bottom contact method. This contact resistance induces the non-Ohmic behavior of I_{ds} at low $|V_{ds}|$ ($\leq$5 V), as shown in panels c and d in Figure 6. The μ values of the CuPc deposited thin-film-based OFETs were reported to be 1.2 $\times$ 10^{-3} to 1.61 $\times$ 10^{-2} cm^2 V^{-1} s^{-1},[39,40] which are lower than those of the β-phase CuPc single rectangular nanotube-based OFETs.

(39) Gao, J.; Xu, J. B.; Zhu, M.; Ke, N.; Ma, D. *J. Phys. D: Appl. Phys.* **2007**, *40*, 5666–5669.
(40) Ofuji, M.; Ishikawa, K.; Takezoe, H.; Inaba, K.; Omote, K. *Appl. Phys. Lett*. **2005**, *86*, 062114−1–062114−3.

Conclusion

The self-assembled CuPc nanowires and their transformed CuPc hollowed rectangular nanotubes have been synthesized in this study. From the FT-IR results, it is suggested that the CF_3COO^- ions interact with the Cu^{2+} ions of the CuPc molecules, and play a bridging role for the self-assembly of the CuPc molecules into a form of nanowires. Through the hydrothermal (followed by the annealing) process, the CuPc nanowires are transformed into the rectangular nanotubes. From the XRD patterns, it is observed that the crystal structure of the CuPc nanowires is α-phase, and that of the CuPc rectangular nanotubes is β-phase and well-alligned along the direction of ($\bar{1}$01). The OFET devices using CuPc nanowires and rectangular nanotubes have been fabricated, and the photoresponsive and gate field-dependent charge transport characteristics have been measured. The ratio of $I_{light/dark}$ of the β-phase CuPc rectangular nanotubes is about 4 times higher than that of the self-assembled α-phase CuPc nanowires. The μ and $I_{on/off}$ of β-phase crystalline CuPc single rectangular nanotube-based OFETs are ~8 and ~10 times higher, respectively, than those of α-phase CuPc single nanowire-based OFETs. These originate from the highly crystalline structure and the relatively strong $\pi-\pi$ interaction of CuPc molecules for the β-phase CuPc nanotubes, supported by the results of HR-TEM, XRD, FT-IR, and UV/vis absorption experiments.

Acknowledgment. This research was supported by Basic Science Research Program through the National Research Foundation of Korea (NRF) funded by the Ministry of Education, Science and Technology (R0A-2007-000-20053-0).

Supporting Information Available: The detailed assignments of the IR characteristic peaks of the self-assembled CuPc nanowires and their hydrothermal and/or annealed nanostructures (PDF). This material is available free of charge via the Internet at http://pubs.acs.org.